NASA TECHNICAL NOTE

NASA TN D-3852

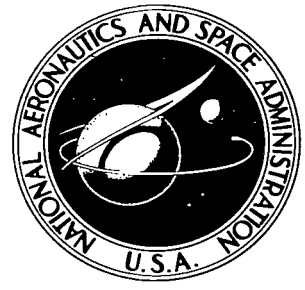

NASA TN D-3852

OFF-DESIGN PERFORMANCE OF TWO ISENTROPIC PLUG NOZZLES DESIGNED FOR A PRESSURE RATIO OF 16.5

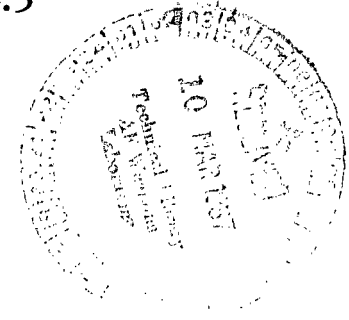

by Bobby L. Berrier and Charles E. Mercer

Langley Research Center
Langley Station, Hampton, Va.

NATIONAL AERONAUTICS AND SPACE ADMINISTRATION • WASHINGTON, D. C. • MARCH 1967

OFF-DESIGN PERFORMANCE OF TWO ISENTROPIC PLUG NOZZLES DESIGNED FOR A PRESSURE RATIO OF 16.5

By Bobby L. Berrier and Charles E. Mercer

Langley Research Center
Langley Station, Hampton, Va.

NATIONAL AERONAUTICS AND SPACE ADMINISTRATION

For sale by the Clearinghouse for Federal Scientific and Technical Information
Springfield, Virginia 22151 – CFSTI price $3.00

OFF-DESIGN PERFORMANCE OF TWO ISENTROPIC PLUG NOZZLES DESIGNED FOR A PRESSURE RATIO OF 16.5

By Bobby L. Berrier and Charles E. Mercer
Langley Research Center

SUMMARY

The performance characteristics of two isentropic plug nozzles installed on a nacelle model have been investigated at static conditions and at Mach numbers of 0.50 to 1.29. Both nozzles were designed to operate at a jet-exit Mach number of 2.46 and a jet total-pressure ratio of 16.5. The ratios of throat critical area to maximum cross-sectional area for the two nozzles were 0.25 and 0.22, and the shroud of the nozzle with the smaller area ratio had a larger shroud lip (more projected area normal to the air-stream). The jet total-pressure ratio was varied from 1.0 to approximately 11.0 depending on the Mach number.

The results indicate that the large-shroud-lip nozzle generally exhibits better internal performance and thrust-minus-drag performance than the small-shroud-lip nozzle although both exhibit poor performance at transonic speeds. The external flow separation on the nozzle boattail is also shown to have a large influence on nozzle performance.

INTRODUCTION

The operation of the supersonic transport airplane and other aircraft in the Mach 3.0 speed range requires engine components which are specifically designed for high-speed flight and which have reasonably good performance for acceleration conditions. Hence, lightweight exhaust nozzles that can provide good thrust characteristics over a wide range of operating pressure ratios are needed. One promising nozzle is the isentropic plug nozzle for which the outer boundary of the exhaust stream continually adjusts to ambient or free-stream pressure. This lightweight nozzle, without the use of variable geometry, has exhibited high thrust performance over a wide range of jet total-pressure ratios in quiescent air (refs. 1 to 3). However, the high pressure ratios inherent for Mach 3.0 aircraft create serious design problems for external expansion, isentropic plug nozzles; that is, the nozzle requires a steep turn at the nozzle throat which results in a nozzle diameter greater than the basic nacelle diameter required by the engine so that a large shroud lip or base is exposed (ref. 4). The short, steep shroud lip, characteristic

of isentropic plug nozzles, induces a sharp turning of the external flow during flight. This flow turning affects the pressures felt on the plug and, thus, offsets some of the good performance at static conditions (ref. 5). At the design pressure ratio and higher supersonic speeds, good performance with this nozzle-plug arrangement has been observed, as indicated by reference 6. However, two-dimensional theory and the results presented in references 5 and 6 show that adverse effects of jet-stream interaction make the performance considerably less at transonic speeds than at static conditions and at supersonic speeds.

Although considerable work on isentropic plug nozzles has been carried out at static conditions and at supersonic speeds, little off-design information is available at transonic speeds for nozzles designed for high pressure-ratio operation. Therefore, the purpose of this investigation was to examine the performance at transonic speeds of an isentropic plug nozzle operating at off-design conditions.

A secondary objective was to obtain information to be used for the correlation of plug-nozzle design parameters at the same design-pressure ratio but for different exhaust fluids. To accomplish this objective, a second nozzle with slightly different geometric parameters was also tested.

The investigation was conducted in the Langley 16-foot transonic tunnel at static conditions and at Mach numbers of 0.50 to 1.29 at zero angle of attack. The jet total-pressure ratio was varied from 1.0 (jet-off) to 11.0 depending on the Mach number. The two nozzles were designed to operate at a jet total-pressure ratio of 16.5 $\left(M_e = 2.46\right)$ for which either the ratio of throat critical area to maximum cross-sectional area or the ratio of projected boattail area to maximum cross-sectional area would be comparable for two fluids having specific-heat ratios of 1.405 and 1.266. The fluid used in the investigation consisted of the decomposition products of hydrogen peroxide and had a specific-heat ratio of 1.266.

SYMBOLS

A_β axially projected cross-sectional area of boattail and base, meters^2

A_e exit area of fully expanded flow, meters^2

A_l local area, meters^2

A_{max} maximum cross-sectional area, meters^2

A_t critical throat area of nozzle, meters^2

$C_{D,\beta}$ boattail pressure drag coefficient, $\sum_{x=0}^{b} -C_p \frac{A_l}{A_{max}}$

where $b = -0.076d_{max}$ for configuration 1
and $b = -0.134d_{max}$ for configuration 2

C_F thrust coefficient, $\frac{F}{q_\infty A_{max}}$

$C_{f,a}$ skin-friction drag coefficient on afterbody, $\frac{\text{Afterbody skin-friction drag}}{q_\infty A_{max}}$

$C_{f,cyl}$ skin-friction drag coefficient on cylindrical part of afterbody, $\frac{\text{Cylinder skin-friction drag}}{q_\infty A_{max}}$

$C_{(F-D)}$ thrust-minus-drag coefficient, $\frac{F - D}{q_\infty A_{max}}$; for static conditions, $\frac{F - D}{p_\infty A_{max}}$

$C_{F,i}$ ideal thrust coefficient, $\frac{F_i}{q_\infty A_{max}}$; for static conditions, $\frac{F_i}{p_\infty A_{max}}$

$C_{F,plug}$ plug thrust coefficient, $\sum_{x/l=0}^{1.0} \frac{C_p A_l}{A_{max}}$

C_p pressure coefficient, $\frac{p_l - p_\infty}{q_\infty}$

$C_{p,a}$ afterbody pressure coefficient, $\left(\frac{p_l - p_\infty}{q_\infty}\right)_{afterbody}$

$C_{p,\beta}$ boattail pressure coefficient, $\left(\frac{p_l - p_\infty}{q_\infty}\right)_{boattail}$

D boattail pressure drag and skin-friction drag, $(C_{D,\beta} + C_{f,a})q_\infty A_{max}$, newtons

d_{max} maximum diameter, meters

F jet thrust, newtons

F_{bal} axial force measured by balance, newtons

F - D thrust minus drag, newtons

F_i ideal thrust for complete isentropic expansion of jet flow, $m\sqrt{2R\frac{\gamma}{\gamma - 1}T_{t,p}\left[1 - \left(\frac{p_\infty}{p_{t,p}}\right)^{\frac{\gamma-1}{\gamma}}\right]}$, newtons

l length of plug from shroud exit, positive downstream, meters

M free-stream Mach number

M_e jet-exit Mach number for fully expanded flow

m mass flow, kilograms/second

p_∞ free-stream or ambient static pressure, newtons/meter^2

p_i internal static pressure, newtons/meter^2

p_l local static pressure, newtons/meter^2

p_{plug} local plug static pressure, newtons/meter^2

$p_{t,p}$ jet total pressure, newtons/meter^2

q_∞ free-stream dynamic pressure, newtons/meter^2

R gas constant, joules/kilogram-^{o}Kelvin

r radius of curvature (see fig. 3), meters

$T_{t,p}$ jet stagnation temperature, ^{o}Kelvin

x axial coordinate from shroud lip, positive downstream (see fig. 3), meters

y radial coordinate (see fig. 3), meters

β external boattail lip angle, degrees

γ ratio of specific heats

θ internal boattail lip angle, degrees

ϕ radial angle of nozzle (see fig. 3), degrees

APPARATUS AND METHODS

Wind Tunnel

The present investigation was conducted in the Langley 16-foot transonic tunnel, which is a single-return, atmospheric wind tunnel with an octagonal test section and continuous air exchange. The tunnel has a continuously variable speed range from a Mach number of 0.20 to 1.30.

Model and Support System

A sketch of the strut-supported, turbojet-engine simulator model used in the investigation is presented in figure 1, and a photograph of the model installed in the test section is given in figure 2. The model consisted of a conical forebody, a cylindrical centerbody of 15.24-cm diameter, and an afterbody-plug combination consisting of a cylindrical section, a boattail, and an isentropic plug. The afterbody-plug combinations were detachable at the 104.39-cm station. The two plug-nozzle combinations investigated were designed on the basis of a computer program adapted from reference 7 for a jet total-pressure ratio of 16.5 (M_e = 2.46) and for the specific-heat ratio γ = 1.266 for hydrogen peroxide. The ratio of throat critical area to maximum cross-sectional area was designed to represent a nonaugmentation condition. The two configurations were also designed to match either the ratio of nozzle throat area to maximum nacelle area of a model which uses air as a working fluid (configuration 1) or the ratio of projected boattail area to maximum nacelle area of a model which uses air as a working fluid (configuration 2). Consideration of these conditions accounts for the small differences between the geometric parameters of the two configurations investigated. Table I gives the basic plug-nozzle designs which further emphasize the differences and similarities of geometric parameters obtained when trying to match the performance of models which use two different exhaust fluids.

A sketch giving dimensions, pressure-orifice locations, and general configuration details is presented in figure 3. A hydrogen peroxide turbojet-engine simulator similar to that described in reference 8 was used for this investigation. The jet simulator produces a hot jet with physical characteristics closely matching the exhaust of a turbojet engine.

TABLE I.- PLUG-NOZZLE DESIGNS

Parameter	Exhaust fluid		
	Air	H_2O_2	
		Configuration 1	Configuration 2
γ	1.405	1.266	1.266
$p_{t,p}/p_\infty$	16.500	16.500	16.500
A_e/A_t	2.570	2.940	2.940
M_e	2.479	2.456	2.456
A_t/A_{max}	.250	.250	.220
A_e/A_{max}	.646	.735	.646
A_β/A_{max}	.354	.265	.354
β, deg	49.583	57.733	49.733
θ, deg	38.617	43.817	43.817
l/d_{max}	.962	.950	.876

Instrumentation

The instrumentation included a one-component, strain-gage thrust balance, measuring gross thrust minus drag of the nozzle, four total-pressure probes (values averaged), and a total-temperature probe located in the tailpipe. Static-pressure orifices were located on the plugs and afterbodies, and a turbine electronic flowmeter was used to measure liquid hydrogen peroxide flow. Pressures were measured with pressure transducers and the electrical signals were transmitted to and recorded by an automatic magnetic tape-recording system.

Data Reduction

The recorded data were used to compute standard force and pressure coefficients. Pressure forces on the shroud lip and the isentropic plug were obtained by assigning to each pressure orifice an incremental area projected on a plane normal to the model axis and by numerically integrating the incremental forces. No correction was made for strut interference because the data from reference 9 indicate that the effect is small for this support system.

The thrust balance measured the sum of the following axial forces: total momentum flux at nozzle throat, plug-pressure forces, external aerodynamic drag of the afterbody aft of station 104.39, some internal tare pressure-area forces in the nacelle, and friction forces. Thrust minus drag for the nozzle was obtained from the following equation:

$$(F - D) = F_{bal} + (p_i - p_\infty)A_{max} + (C_{f,cyl})q_\infty A_{max}$$

To obtain internal performance, which includes total momentum flux at the nozzle throat plus plug forces, the following equation was used:

$$F = (F - D) + D$$

Tests

Both configurations were investigated at static conditions and at Mach numbers from 0.50 to 1.29. The angle of attack was held at a constant value of 0^o during the entire investigation. The ratio of jet total pressure to free-stream static pressure was varied from 1.0 (jet off) to about 11.0. The average Reynolds number based on body length was 18.5×10^6.

RESULTS AND DISCUSSION

Afterbody Pressure and Drag

Figures 4 and 5 show, respectively, the jet-off and jet-on pressure distributions on the external surface of the two afterbodies for various Mach numbers. Pressures were measured around the boattail at 0^o, 180^o, and 270^o locations but are presented in figures 4 and 5 as an average. Both configurations show an abrupt decrease in pressure over the external lip with the flow becoming separated (depending on jet total-pressure ratio) as shown in figure 5. This separation is typical for afterbodies having large boattail angles (table I), as emphasized by the pressure distributions presented in reference 10.

Figure 5 shows that increasing jet total-pressure ratio decreased the pressures around the afterbodies for all Mach numbers. This decrease is due to the jet's either aspirating the separated boattail region to very low pressure coefficients (see ref. 10) or reducing the amount of separation. For a Mach number of 1.00 or above, the highest jet total-pressure ratio tended to increase the pressure coefficients on the boattails. This increase is due to the expansion of the jet plume into the free-stream flow which reduces the aspiration effects of the jet. The decrease of the pressures on the cylindrical portion of the afterbodies is less pronounced at the higher Mach numbers since disturbances can be propagated only a short distance upstream through the boundary layer at these speeds.

The pressures presented in figures 4 and 5 were integrated over the axially projected boattail to obtain the boattail pressure drag values presented in figures 6 and 7. The variation of boattail drag with Mach number for jet-off conditions is shown in figure 6. In the region $1.05 < M < 1.13$, some interference from shock waves reflected from the wall may be present, although none is apparent for the data presented in figure 6.

The boattail drag level of configuration 2 (large shroud lip) is higher than that of configuration 1 for all Mach numbers, primarily because of a larger projected area.

The effects of jet operation on boattail drag are presented in figure 7. At subsonic speeds, jet operation increases the boattail drag of both configurations. At sonic and low supersonic speeds, a hysteresis effect is exhibited as jet total-pressure ratio is varied continuously (being increased and then decreased). This effect is attributed to the axial movement of the flow separation point on the boattail. With decreasing jet total-pressure ratio (indicated by arrows), the upstream movement of the separation point and the attendant decrease in drag was delayed to a lower value of $p_{t,p}/p_\infty$ than that associated with the initial boattail drag rise with increasing $p_{t,p}/p_\infty$. The boattail drag coefficients indicate that the flow became attached at lower values of jet total-pressure ratio for configuration 1 (small shroud lip) than for configuration 2, with an exception noted at $M = 1.29$.

In general, the large increase in boattail drag observed in figure 7 was delayed on configuration 2 (particularly at $M = 1.00$) until a higher value of jet total-pressure ratio was obtained than that obtained for configuration 1. Both figures 5 and 7 emphasize a large detrimental effect of jet operation at transonic Mach numbers on the lip pressures and drag.

Pressure Distribution and Thrust on Isentropic Plug

The plug pressure distributions for several Mach numbers and several jet total-pressure ratios are presented in figure 8. These plug pressure distributions are typical of plug-type nozzles (refs. 5, 11, and 12). Generally, the plug pressures for both configurations remained above the free-stream value. This pressure difference adds a beneficial thrust term to the nozzle performance.

The variation in plug thrust coefficient with jet total-pressure ratio and Mach number is presented in figure 9. The plug thrust was obtained by integrating the pressures shown in figure 8 over the axially projected plug area. Note that at a Mach number of zero $C_{F,plug}$ is the plug pressure force divided by ambient pressure rather than by free-stream dynamic pressure q_∞, as for Mach numbers greater than zero.

Positive plug thrust was obtained, as indicated by the plug pressures of figure 8, for both configurations throughout the Mach number range except at transonic and low supersonic speeds for jet total-pressure ratios less than 2.8. Configuration 2 has higher values of plug thrust than configuration 1 except for Mach numbers of 0.50 or less. The slope of the plug-thrust curve decreases with increasing Mach number; however, the plug thrust remains at approximately the same percentage of the total thrust for all Mach numbers. Figure 9 shows that for supersonic speeds and at pressure ratios typical for a turbojet engine, the plug thrust $C_{F,plug}$ is approximately equal to the boattail pressure

drag coefficient $C_{D,\beta}$ of figure 7. As a result, the lip drag cancels the plug thrust and only the throat thrust is available for propulsive forces.

Nozzle Performance Characteristics

Basic data.- Figure 10 presents the static thrust-minus-drag coefficient and the ideal static thrust coefficient as functions of jet total-pressure ratio for the two configurations tested. These static coefficients are defined as the thrust force divided by ambient pressure p_∞ and the reference area A_{max}.

Thrust-minus-drag coefficients, thrust coefficients, and ideal thrust coefficients for both configurations are shown for several Mach numbers and jet total-pressure ratios in figures 11 and 12. These coefficients are defined as the thrust-minus-drag force or thrust force (measured or ideal) divided by free-stream dynamic pressure q_∞ and the reference area A_{max}. These values are much lower than those obtained on an isentropic plug nozzle with a boattail angle of 10.5° and design pressure ratio of 10 (ref. 13), but they exhibit similar trends. The results in reference 14 indicate that the transonic performance could be improved with the addition of terminal fairings, which thus offer a possible solution for the low transonic performance typical for isentropic plug nozzles.

Thrust-minus-drag ratio.- The variation of thrust-minus-drag ratio with jet total-pressure ratio and Mach number is presented in figure 13. The thrust-minus-drag ratio increased with increasing jet total-pressure ratio for all Mach numbers and a maximum value of $(F - D)/F_i$ was not obtained for either configuration. The performance of both configurations for a constant value of jet total-pressure ratio decreased with increasing Mach number.

At subsonic speeds, the nozzle with the large shroud lip (configuration 2) had higher performance throughout the entire range of jet total-pressure ratios tested. At transonic and low supersonic speeds, external flow separation on the boattails had a large effect on thrust-minus-drag performance. A hysteresis effect, which is due to the axial movement of the separation point on the boattail discussed in the section entitled "Afterbody Pressure and Drag," is exhibited in figure 13 for $1.0 \leq M \leq 1.29$. Hence thrust-minus-drag performance characteristics of both nozzles in this speed regime are a function of the flow stability parameters (for example, Reynolds number, temperature of wall, wall surface condition, jet total-pressure ratio, boattail angle).

Internal performance.- The variation of internal performance F/F_i with jet total-pressure ratio and Mach number is presented in figure 14. The internal performance of the large-lip nozzle (configuration 2) was generally better than that of the small-lip nozzle (configuration 1) for all Mach numbers. Note that external flow separation does not affect internal performance and hence no hysteresis effects are present, as in figure 13.

The internal performance of both configurations increased with increasing jet total-pressure ratio at all Mach numbers.

Performance at a scheduled pressure ratio.- The variation of nozzle internal performance and gross thrust-minus-drag ratio with Mach number for a typical turbojet total-pressure-ratio schedule is presented in figure 15. Gross thrust-minus-drag ratio decreased with increasing Mach number for both configurations throughout the subsonic speed range, but the large-shroud-lip nozzle (configuration 2) had the best performance.

At sonic and low supersonic speeds, configuration 1 incurred much higher losses than configuration 2, except at $M = 1.29$. These losses occurred because the external flow remained attached to a larger portion of the boattail of configuration 1 than of configuration 2 for the given turbojet total-pressure-ratio schedule. It should be noted that the use of a decreasing pressure-ratio schedule necessary for decreasing speed would present a lower level of thrust-minus-drag performance for configuration 2 because the flow remains attached to a larger portion of the boattail until lower jet total-pressure ratios are reached. Comparison of the thrust-minus-drag performance of configuration 2 with that of the nozzle investigated in reference 5 (subsonic experimental data and supersonic two-dimensional theory) shows a loss of about 2.5 percent in the subsonic range and mixed results in the supersonic range. These results are considered to be in good agreement, as the performance level of reference 5 is slightly high because of the use of ideal thrust rather than actual measured thrust for obtaining nozzle performance.

The internal performance of the large-shroud-lip nozzle (configuration 2) remained higher than that of the small-shroud-lip nozzle (configuration 1) throughout the Mach number range. The internal performance of both configurations decreased for $M < 1.0$ and increased for $M > 1.0$ with increasing Mach number. The internal performance of configuration 2 is lower than that of the configuration of reference 5; however, if the data of reference 5 were corrected for the amount that quiescent-air thrust would be below ideal thrust, fairly good agreement for this speed range would result.

In general, both fixed-geometry, isentropic plug nozzles exhibited poor performance at transonic speeds and, thus, illustrate that fixed-geometry, isentropic plug nozzles operating at off-design conditions create large losses in performance. These large losses tend to offset any advantages that fixed-geometry, isentropic plug nozzles might have because of nozzle simplicity and a reduction in weight.

CONCLUDING REMARKS

An investigation of the performance of two isentropic plug nozzles, designed for a jet total-pressure ratio of 16.5 and for ratios of nozzle throat area A_t to maximum cross-sectional area A_{max} of 0.25 and 0.22 for configurations 1 and 2, respectively,

at off-design operating conditions at Mach numbers up to 1.29, jet total-pressure ratios up to 11.0, and an angle of attack of 0^{o}, indicated the following trends:

1. The large-shroud-lip nozzle (configuration 2) had generally better internal performance and thrust-minus-drag performance than the small-shroud-lip nozzle (configuration 1) for the Mach number range and the given typical turbojet total-pressure-ratio schedule.

2. Jet total-pressure ratio and Mach number affected the initiation of afterbody flow separation which induced large effects on nozzle performance.

3. Both fixed-geometry, isentropic plug nozzles designed for a jet total-pressure ratio of 16.5 exhibited poor performance at transonic speeds.

Langley Research Center,
National Aeronautics and Space Administration,
Langley Station, Hampton, Va., October 6, 1966,
720-03-01-01-23.

REFERENCES

1. Krull, H. George; and Beale, William T.: Effect of Plug Design on Performance Characteristics of Convergent-Plug Exhaust Nozzles. NACA RM E54H05, 1954.

2. Krull, H. George; and Beale, William T.: Effect of Outer-Shell Design on Performance Characteristics of Convergent-Plug Exhaust Nozzles. NACA RM E54K22, 1955.

3. Krull, H. George; Beale, William T.; and Schmiedlin, Ralph F.: Effect of Several Design Variables on Internal Performance of Convergent-Plug Exhaust Nozzles. NACA RM E56G20, 1956.

4. Runckel, Jack F.: Review of NASA Exhaust Nozzle Research. Proceedings of NASA Conference on Supersonic-Transport Feasibility Studies and Supporting Research. NASA TM X-905, 1963, pp. 315-332.

5. Salmi, Reino J.; and Cortright, Edgar M., Jr.: Effects of External Stream Flow and Afterbody Variations on the Performance of a Plug Nozzle at High Subsonic Speeds. NACA RM E56F11a, 1956.

6. Valerino, Alfred S.; Zappa, Robert F.; and Abdalla, Kaleel L.: Effects of External Stream on the Performance of Isentropic Plug-Type Nozzles at Mach Numbers of 2.0, 1.8, and 1.5. NASA MEMO 2-17-59E, 1959.

7. Connors, James F.; and Meyer, Rudolph C.: Design Criteria for Axisymmetric and Two-Dimensional Supersonic Inlets and Exits. NACA TN 3589, 1956.

8. Runckel, Jack F.; and Swihart, John M.: A Hydrogen Peroxide Hot-Jet Simulator for Wind-Tunnel Tests of Turbojet-Exit Models. NASA MEMO 1-10-59L, 1959.

9. Norton, Harry T., Jr.; Runckel, Jack F.; and Pendergraft, Odis C., Jr.: Transonic Performance of Two Convergent-Divergent Ejector Nozzles Designed for Corrected Secondary Flows of 3 and 9.4 Percent. NASA TM X-909, 1964.

10. Henry, Beverly Z., Jr.; and Cahn, Maurice S.: Pressure Distributions Over a Series of Related Afterbody Shapes As Affected by a Propulsive Jet at Transonic Speeds. NACA RM L56K05, 1957.

11. Schmeer, James W.; Kirkham, Frank S.; and Salters, Leland B., Jr.: Performance Characteristics of a 10^{o} Conical Plug Nozzle at Mach Numbers up to 1.29. NASA TM X-913, 1964.

12. Angelino, G.: Theoretical and Experimental Investigation of the Design and Performance of a Plug-Type Nozzle. Tech. Note 12, Training Center Exptl. Aerodyn. (Belgium), July 1963.

13. Willis, Conrad M.; and Norton, Harry T., Jr.: Effect of Afterbody Terminal Fairings on the Performance of Plug-Type Exhaust Nozzles at Transonic Speeds. NASA TM X-762, 1963.

14. Mercer, Charles E.; and Salters, Leland B., Jr.: Performance of a Plug Nozzle Having a Concave Central Base With and Without Terminal Fairings at Transonic Speeds. NASA TN D-1804, 1963.

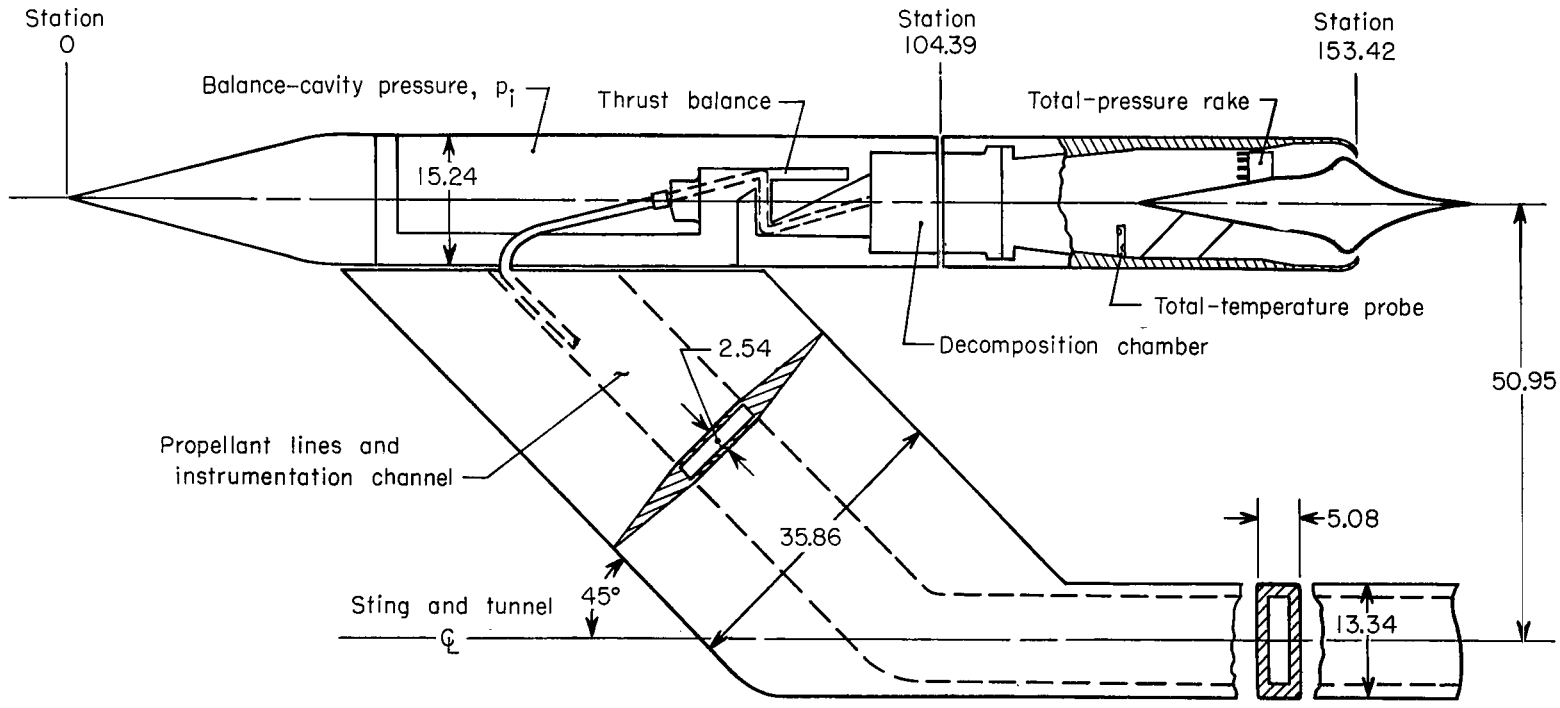

Figure 1.- Sketch of isentropic plug nozzle installed on a nacelle model. All dimensions are in centimeters.

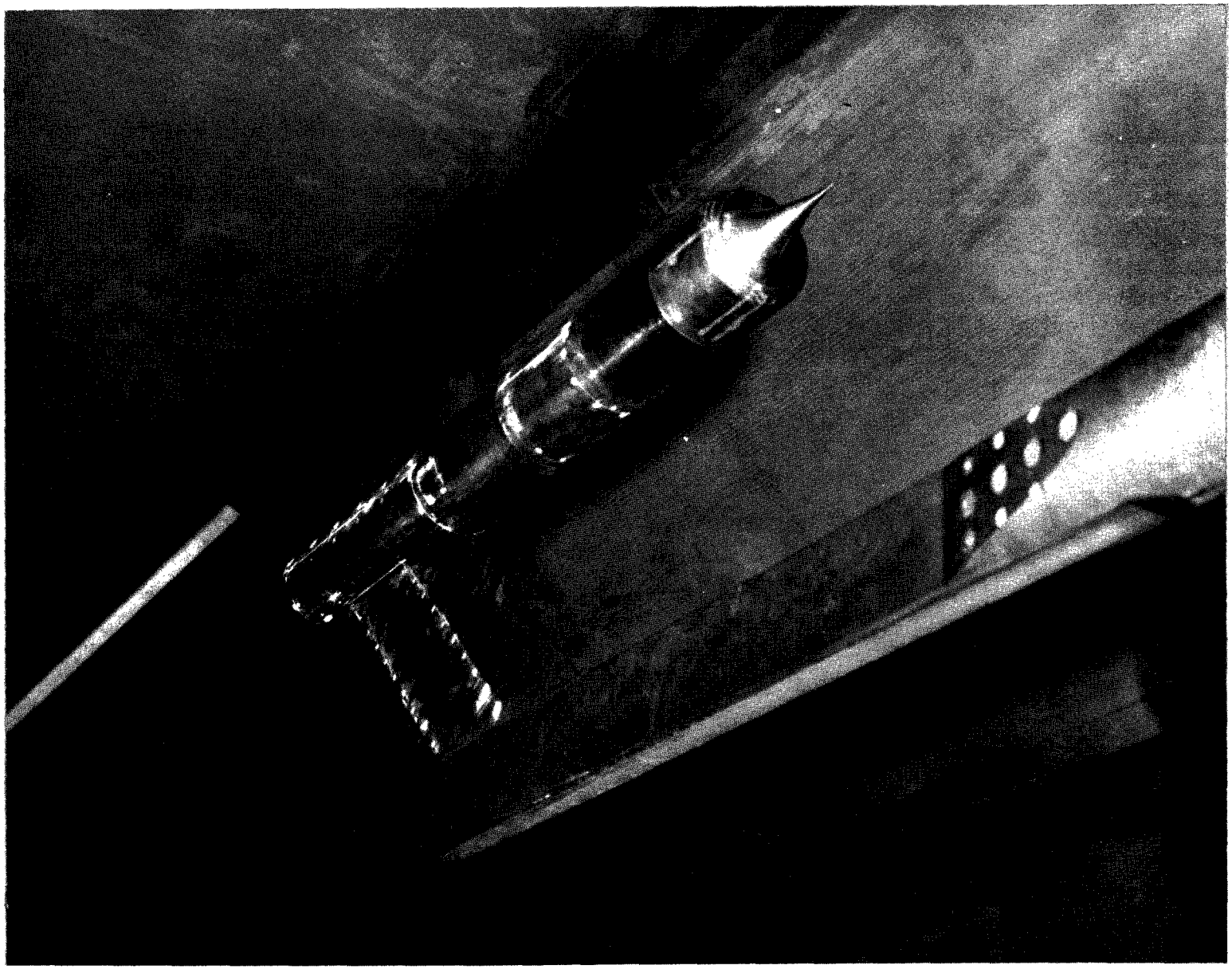

Figure 2.- Photograph of isentropic plug nozzle, configuration 1, mounted on a nacelle model. L-65-1453

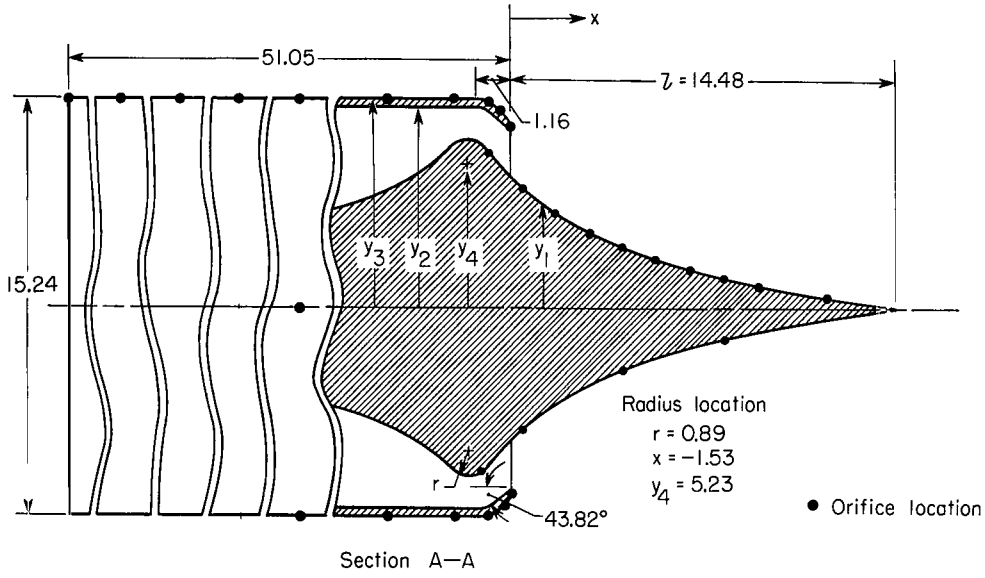

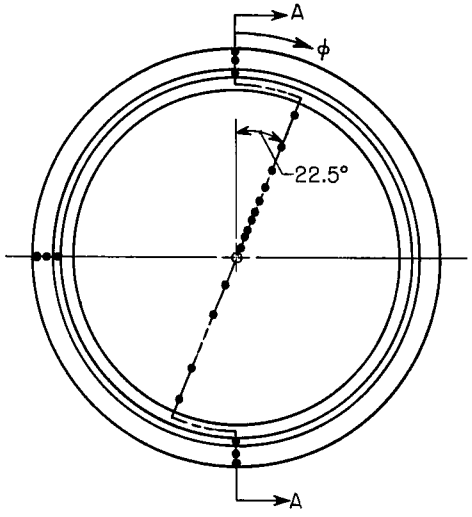

Isentropic plug-nozzle coordinates					
x	y_1	y_2	y_3	x	y_1
−51.1	——	——	7.62	1.0	3.97
−5.5	3.94	7.37	7.62	1.5	3.63
−4.5	4.33	7.37	7.62	2.0	3.34
−3.5	4.82	7.37	7.62	3.0	2.82
−2.5	5.53	7.37	7.62	4.0	2.39
−2.0	5.99	7.37	7.62	5.0	2.01
−1.5	6.12	7.37	7.62	6.0	1.66
−1.0	5.96	7.35	7.61	7.5	1.23
−0.5	5.35	7.05	7.40	9.0	.88
0	4.78	6.53	6.79	10.5	.56
.5	4.34	——	——	12.0	.30
				13.8	.08

Orifice locations			
Isentropic plug		Afterbody	
ϕ, deg	x	ϕ, deg	x
202.5	−1.09	0, 180, and 270	0
22.5	−0.84	0, 180, and 270	−0.30
22.5 and 202.5	.43	0, 180, and 270	−0.91
22.5	1.70	0, 180, and 270	−2.13
22.5	2.97	0, 180, and 270	−4.72
22.5 and 202.5	4.24	0, 180, and 270	−9.75
22.5	5.51	0	−19.20
22.5	6.78	0	−33.68
22.5 and 202.5	8.05	0	−41.45
22.5	9.32	0	−51.05
22.5	11.86		

(a) Configuration 1.

Figure 3.- Sketch of plug-nozzle configurations. All dimensions in centimeters.

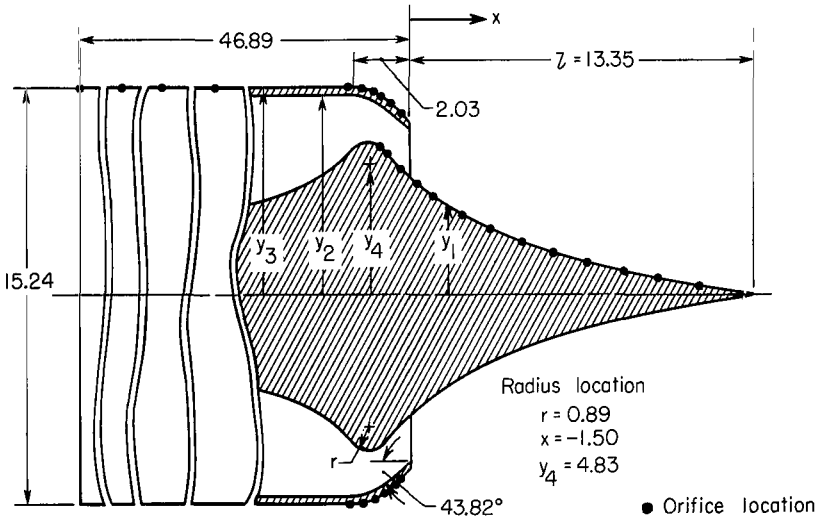

Section A—A

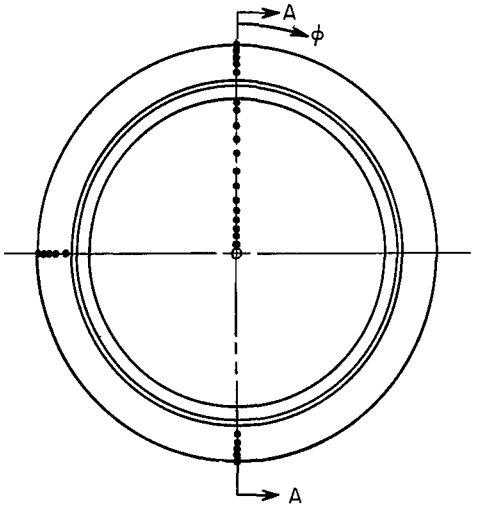

Isentropic plug-nozzle coordinates					
x	y_1	y_2	y_3	x	y_1
−46.9	—	—	7.62	1.5	3.30
−5.5	3.53	7.37	7.62	2.0	3.02
−4.5	3.84	7.37	7.62	3.0	2.54
−3.5	4.23	7.37	7.62	4.0	2.14
−2.5	5.02	7.37	7.62	5.0	1.78
−2.0	5.57	7.34	7.62	6.0	1.45
−1.5	5.72	7.23	7.54	7.5	1.02
−1.0	5.58	6.96	7.28	9.0	.69
−0.5	4.99	6.58	6.86	10.5	.41
0	4.43	6.13	6.30	12.0	.20
.5	4.00	—	—	12.8	.07
1.0	3.63	—	—		

Orifice locations			
Isentropic plug		Afterbody	
ϕ, deg	x	ϕ, deg	x
0	−1.07	0, 180, and 270	−0.30
0	−0.81	0, 180, and 270	−0.64
0	−0.25	0, 180, and 270	−0.96
0	.28	0, 180, and 270	−1.27
0	.91	0, 180, and 270	−1.78
0	2.03	0, 180, and 270	−2.29
0	3.20	0	−15.24
0	4.37	0	−29.72
0	5.56	0	−37.24
0	6.86	0	−46.89
0	8.28		
0	9.58		
0	11.23		

(b) Configuration 2.

Figure 3.- Concluded.

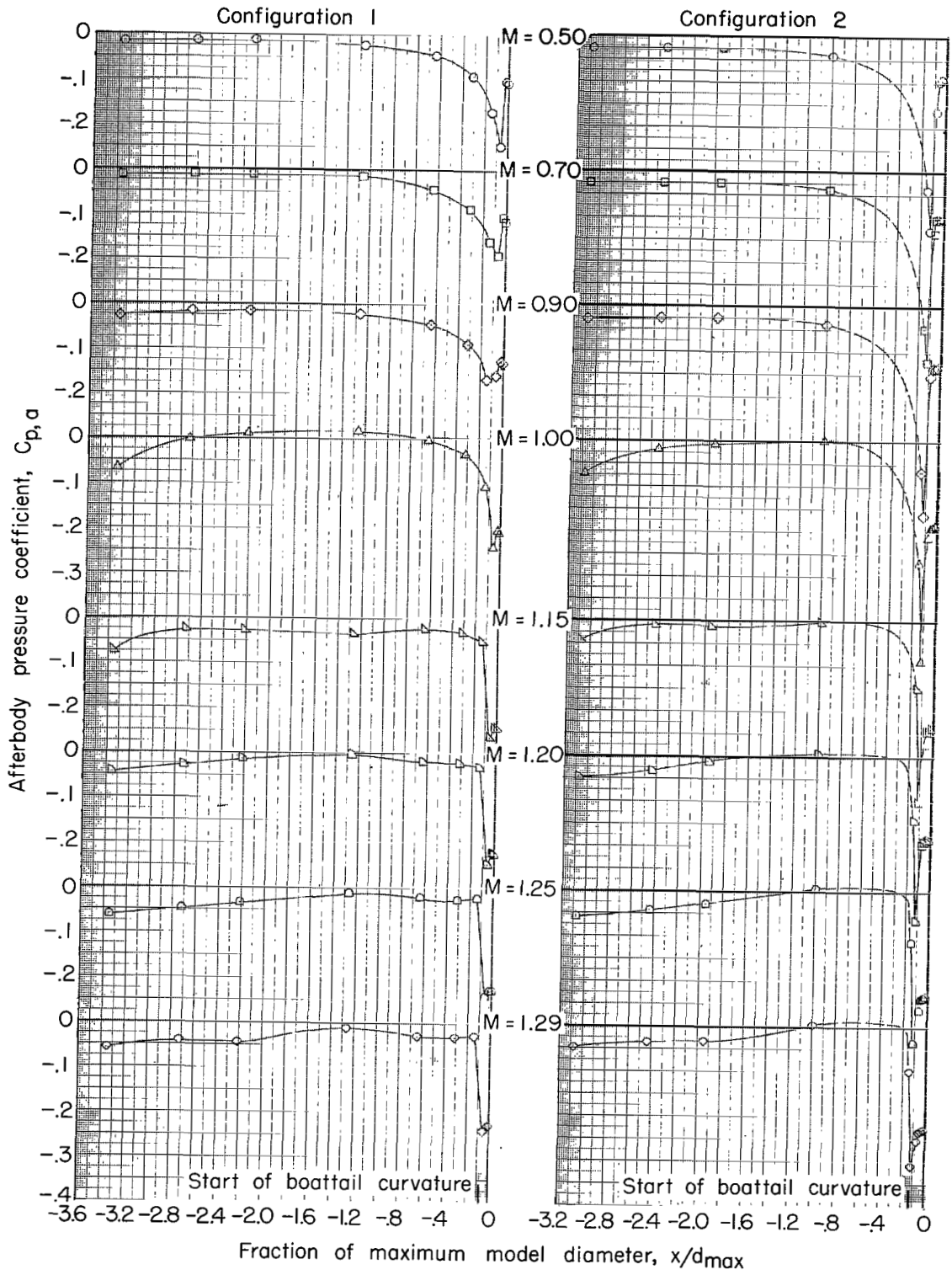

Figure 4.- Effect of Mach number on external pressure distributions. Jet off.

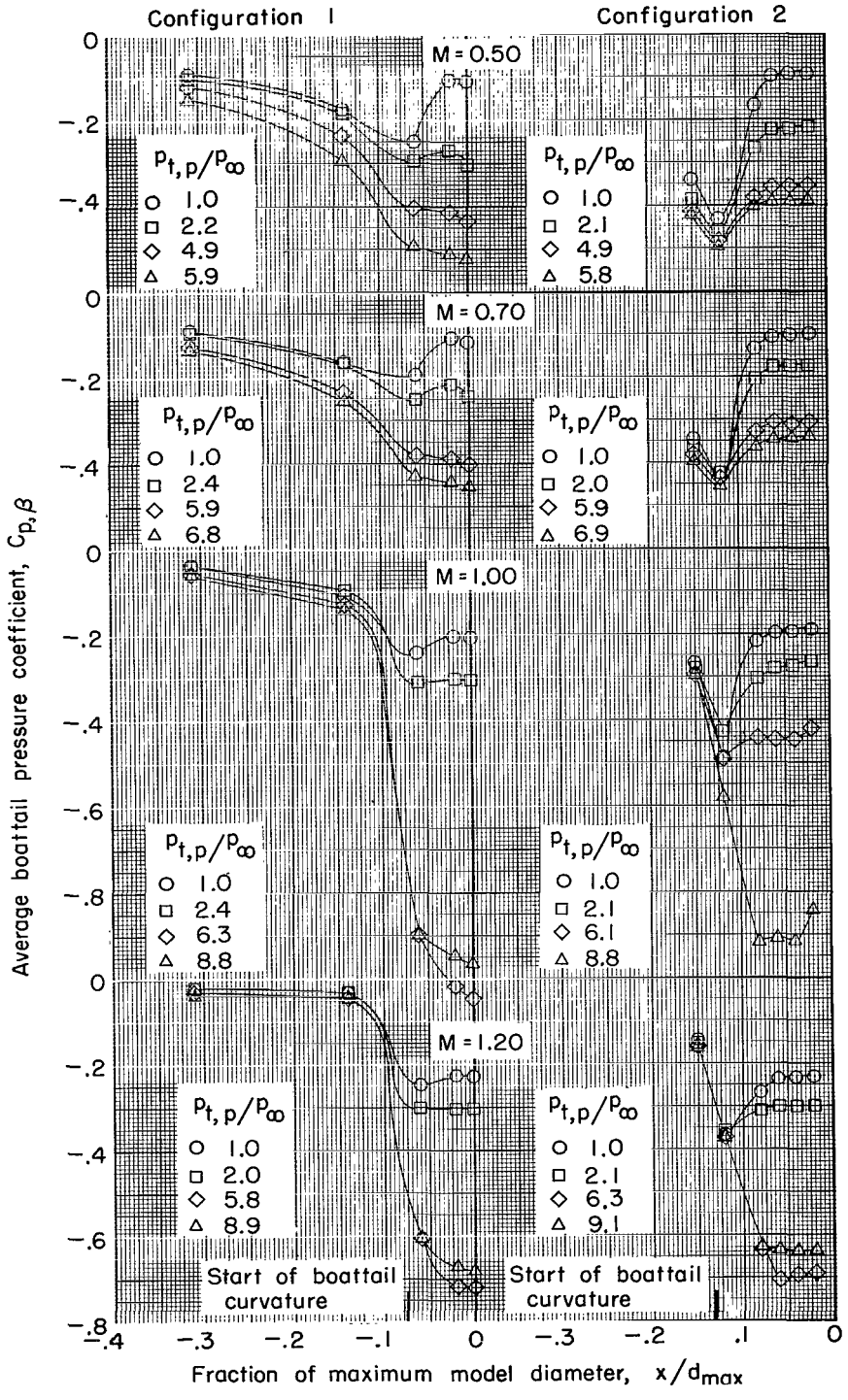

Figure 5.- Effect of jet total-pressure ratio on boattail pressure distributions for various Mach numbers.

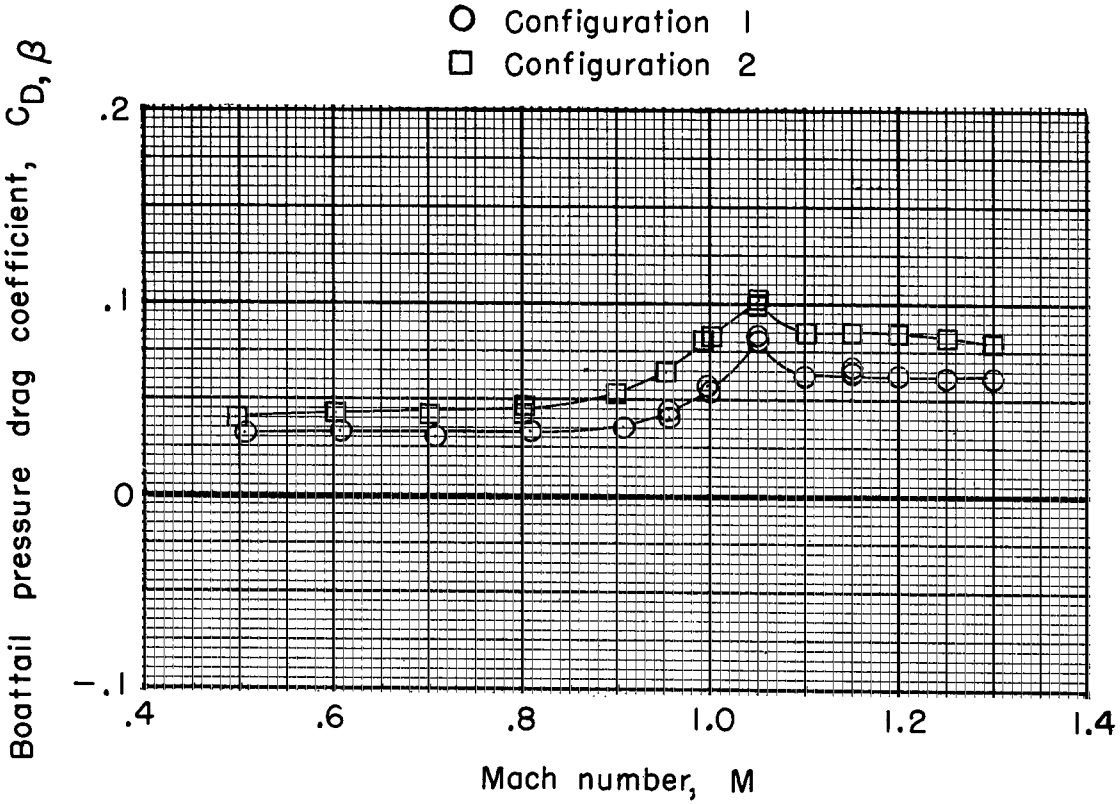

Figure 6.- Variation of boattail drag coefficient with Mach number for jet-off conditions.

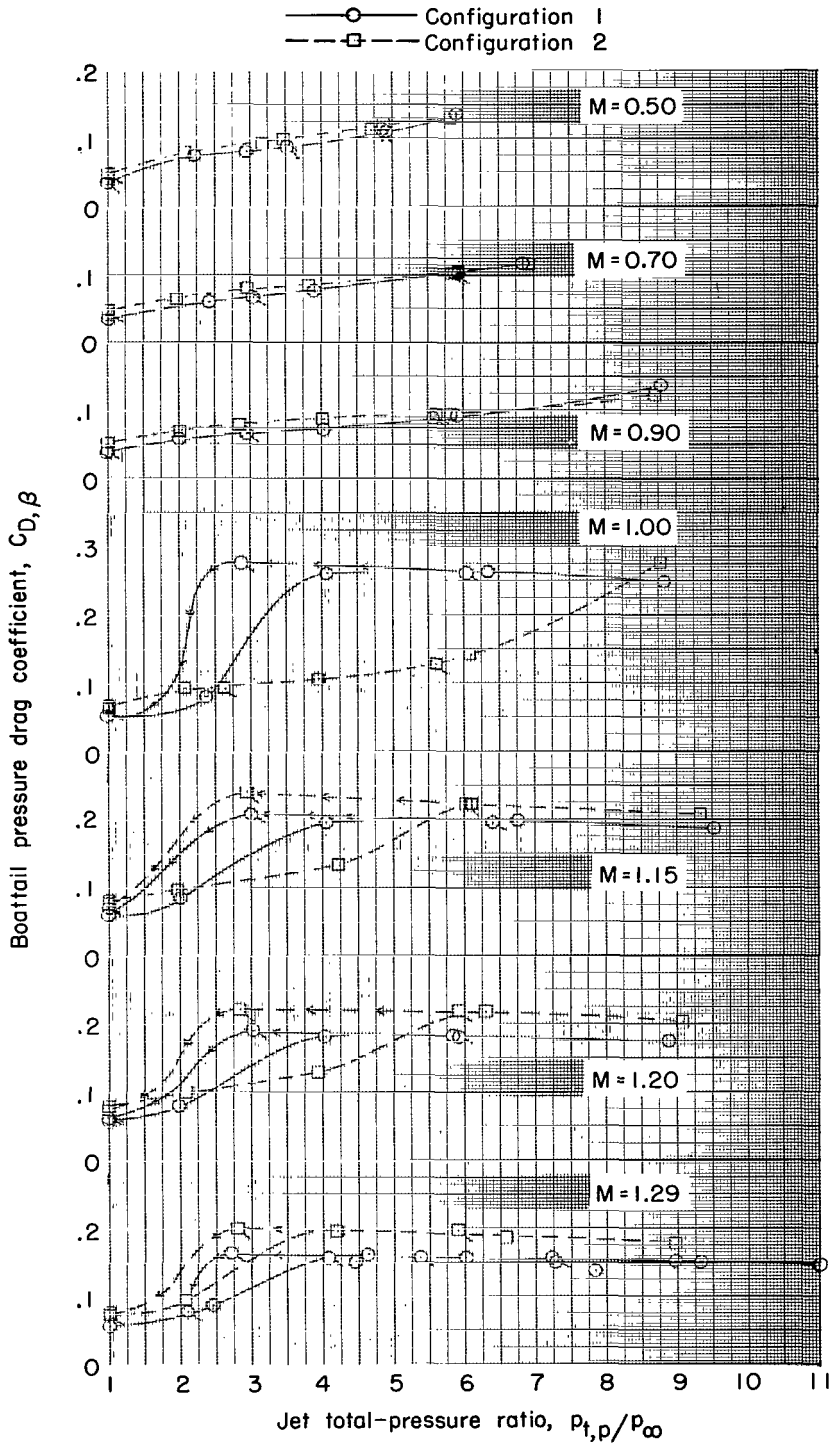

Figure 7.- Variation of boattail drag coefficient with jet total-pressure ratio. Flagged symbols denote decreasing pressure ratios.

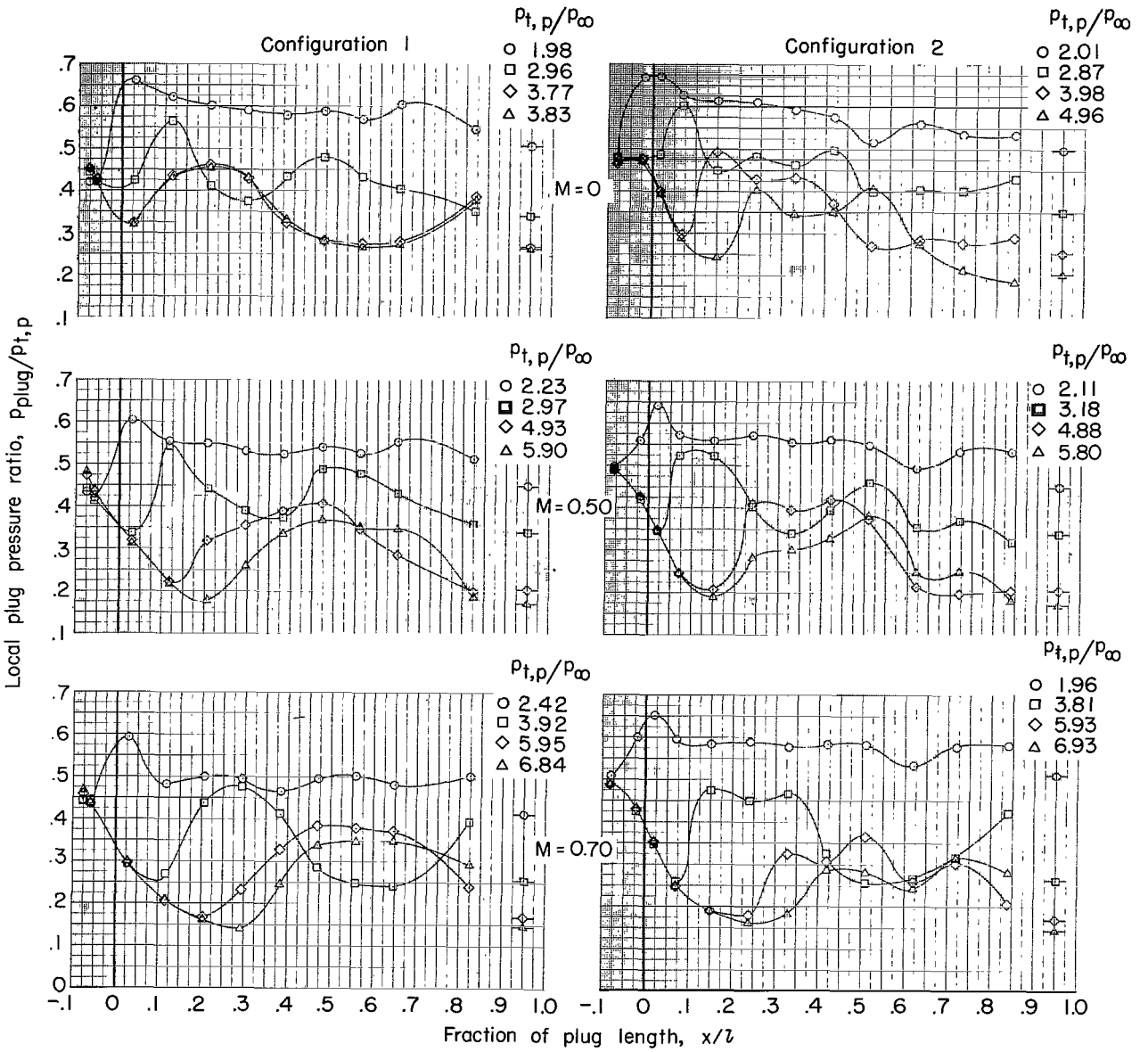

(a) M = 0 to 0.70.

Figure 8.- Effect of jet total-pressure ratio on plug pressure distributions for various Mach numbers. Isolated symbols with ticks indicate values of $p_\infty/p_{t,p}$.

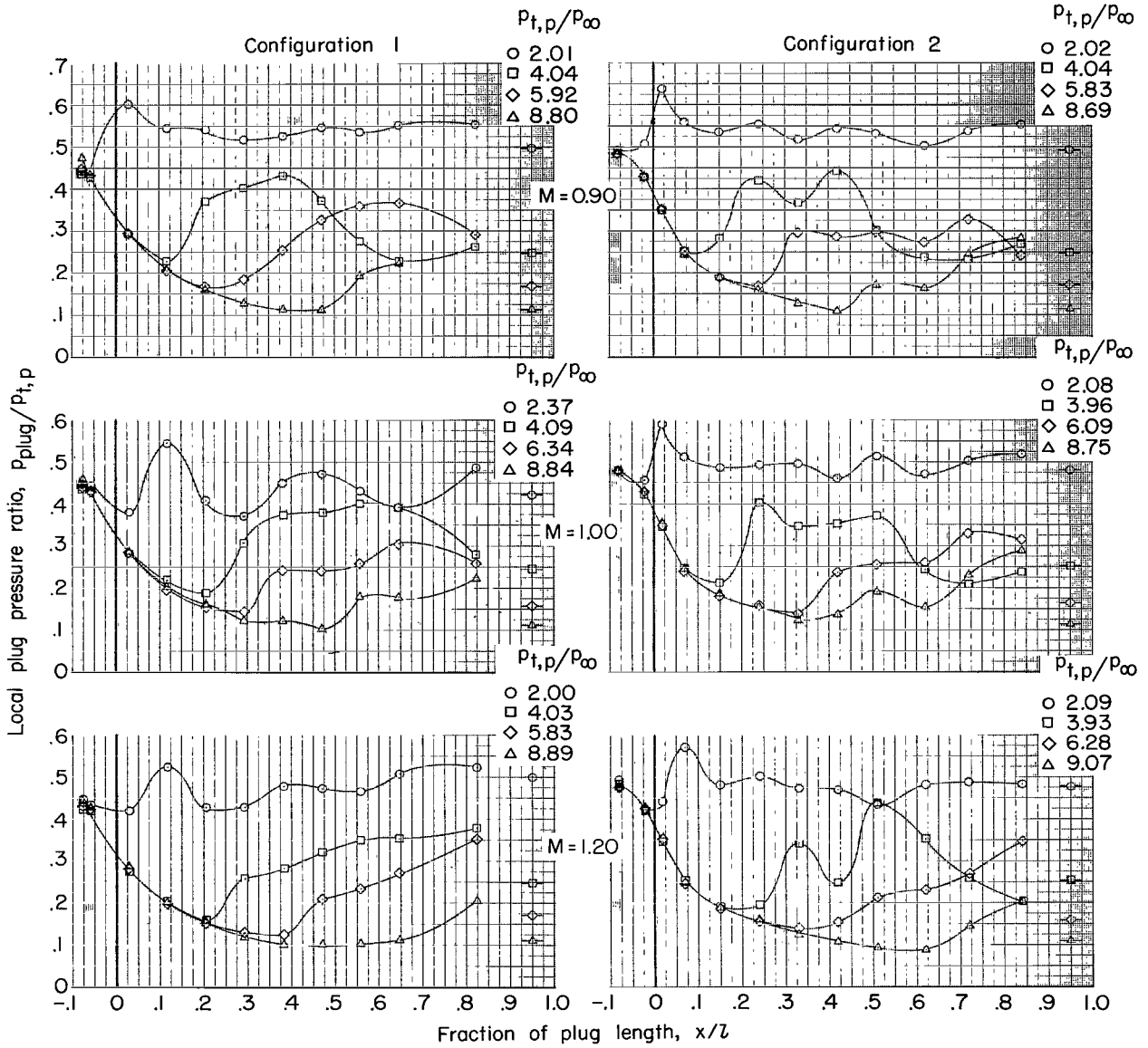

(b) M = 0.90 to 1.20.

Figure 8.- Concluded.

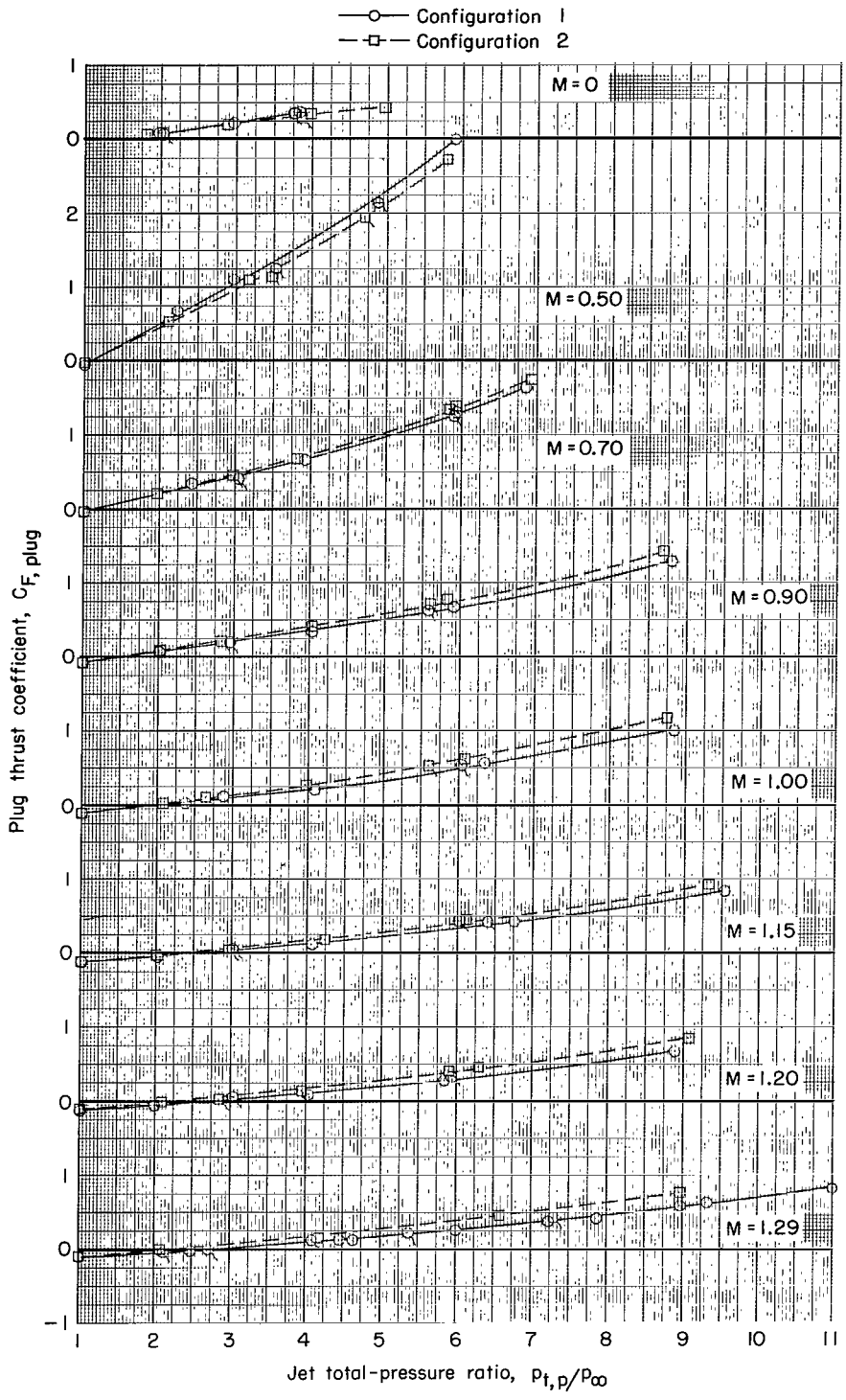

Figure 9.- Variation of plug thrust coefficient with jet total-pressure ratio and Mach number. Flagged symbols indicate decreasing pressure ratios.

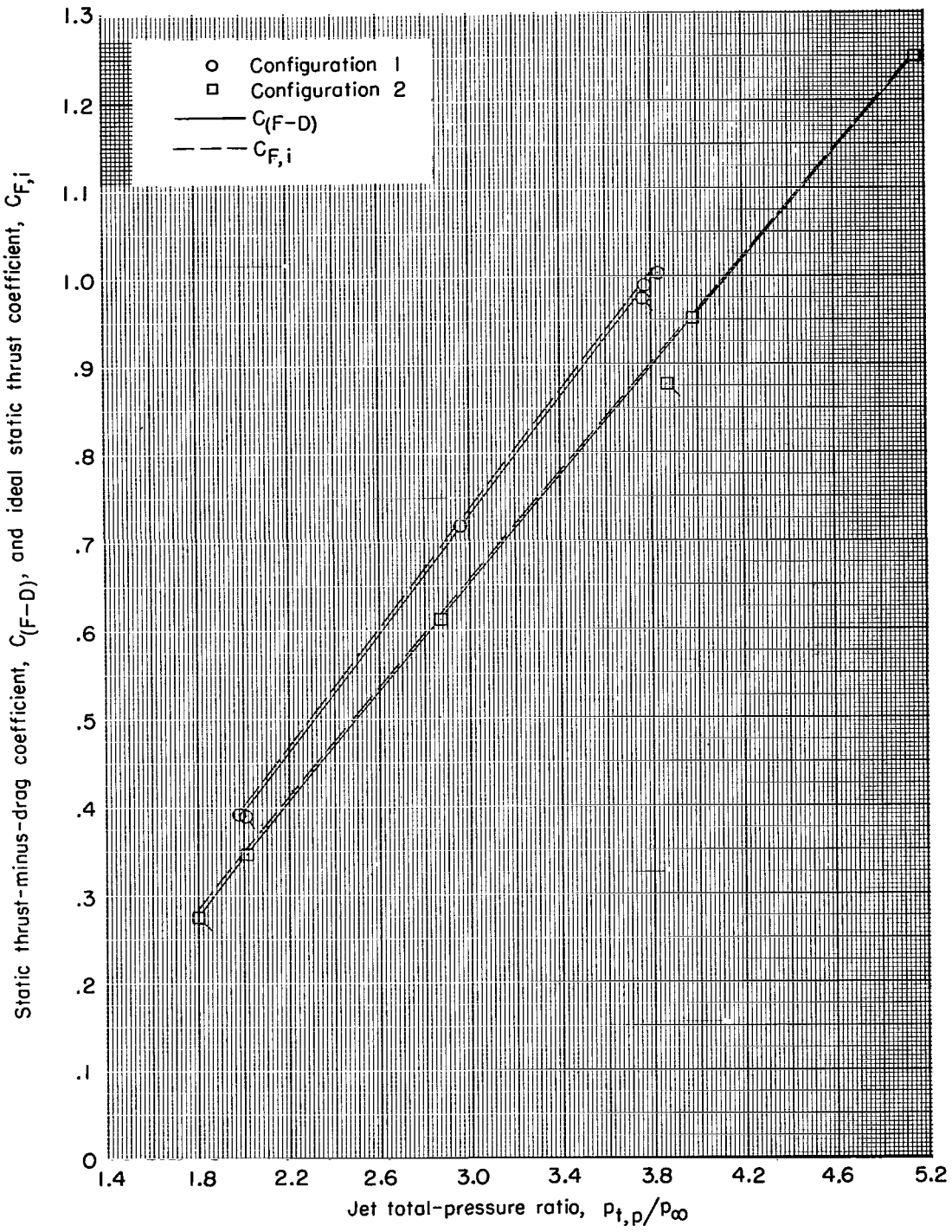

Figure 10.- Variation of static thrust-minus-drag coefficient and ideal static thrust coefficient with jet total-pressure ratio. Flagged symbols indicate decreasing pressure ratios.

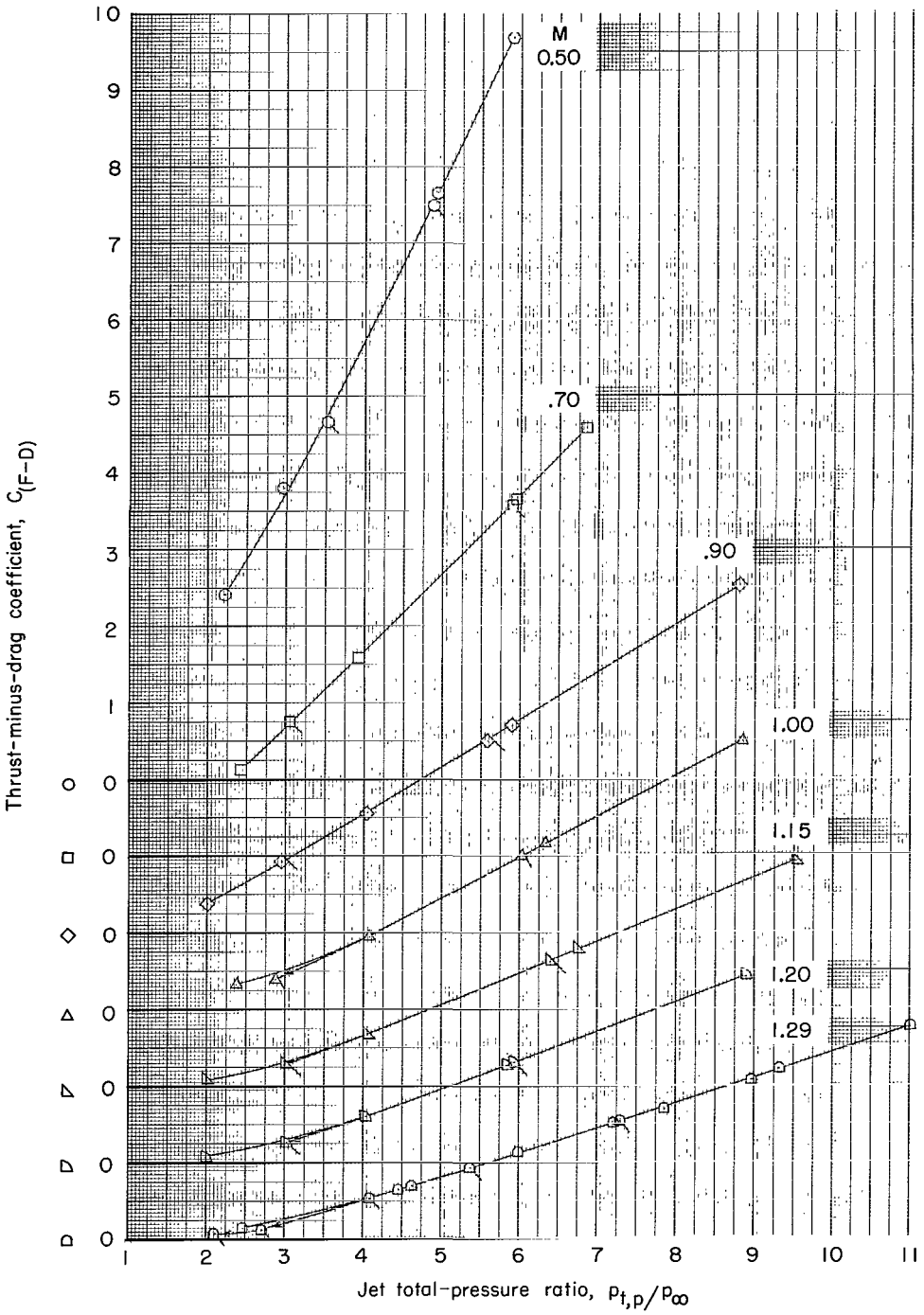

(a) Configuration 1.

Figure 11.- Variation of thrust-minus-drag coefficient with jet total-pressure ratio for various Mach numbers. Flagged symbols indicate decreasing pressure ratios. (Note shifting scales.)

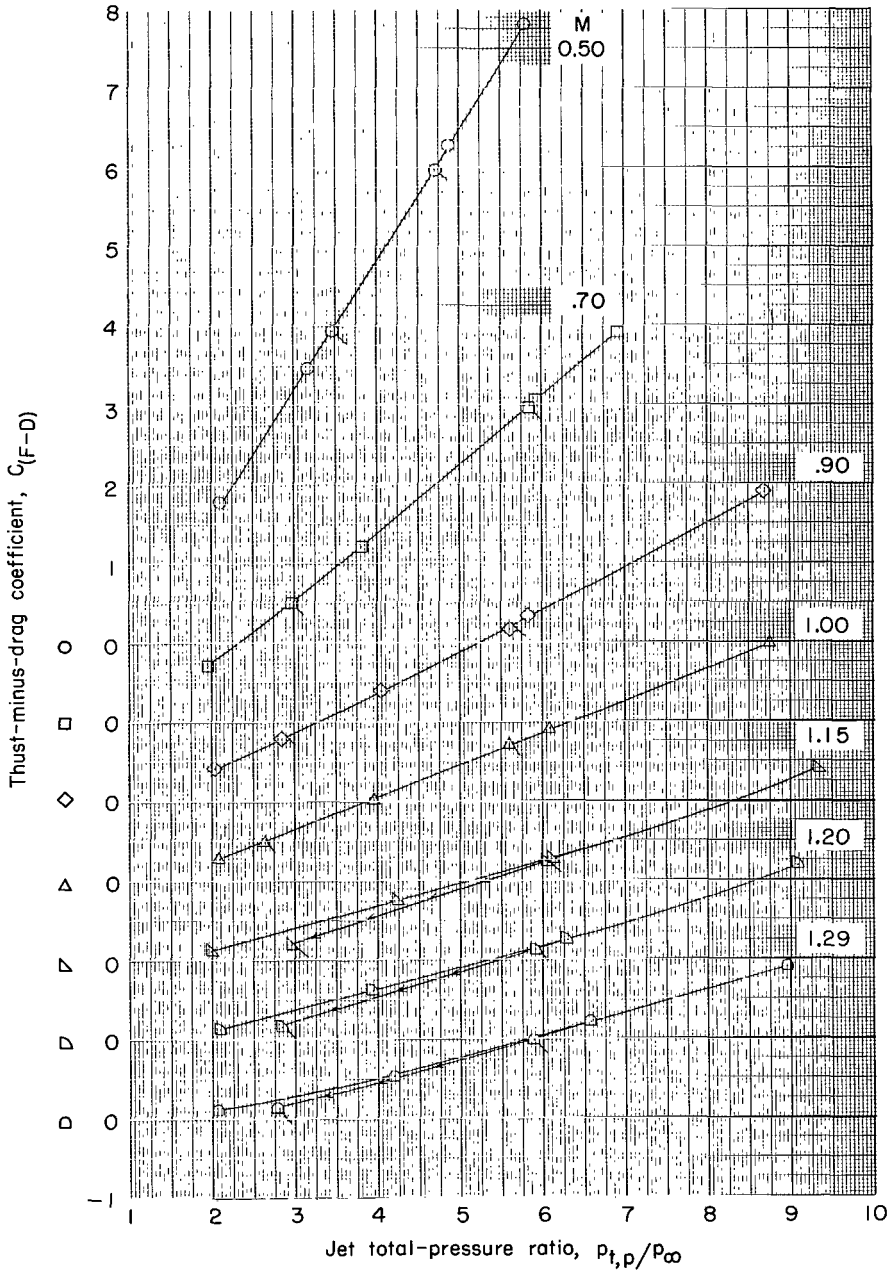

(b) Configuration 2.

Figure 11.- Concluded.

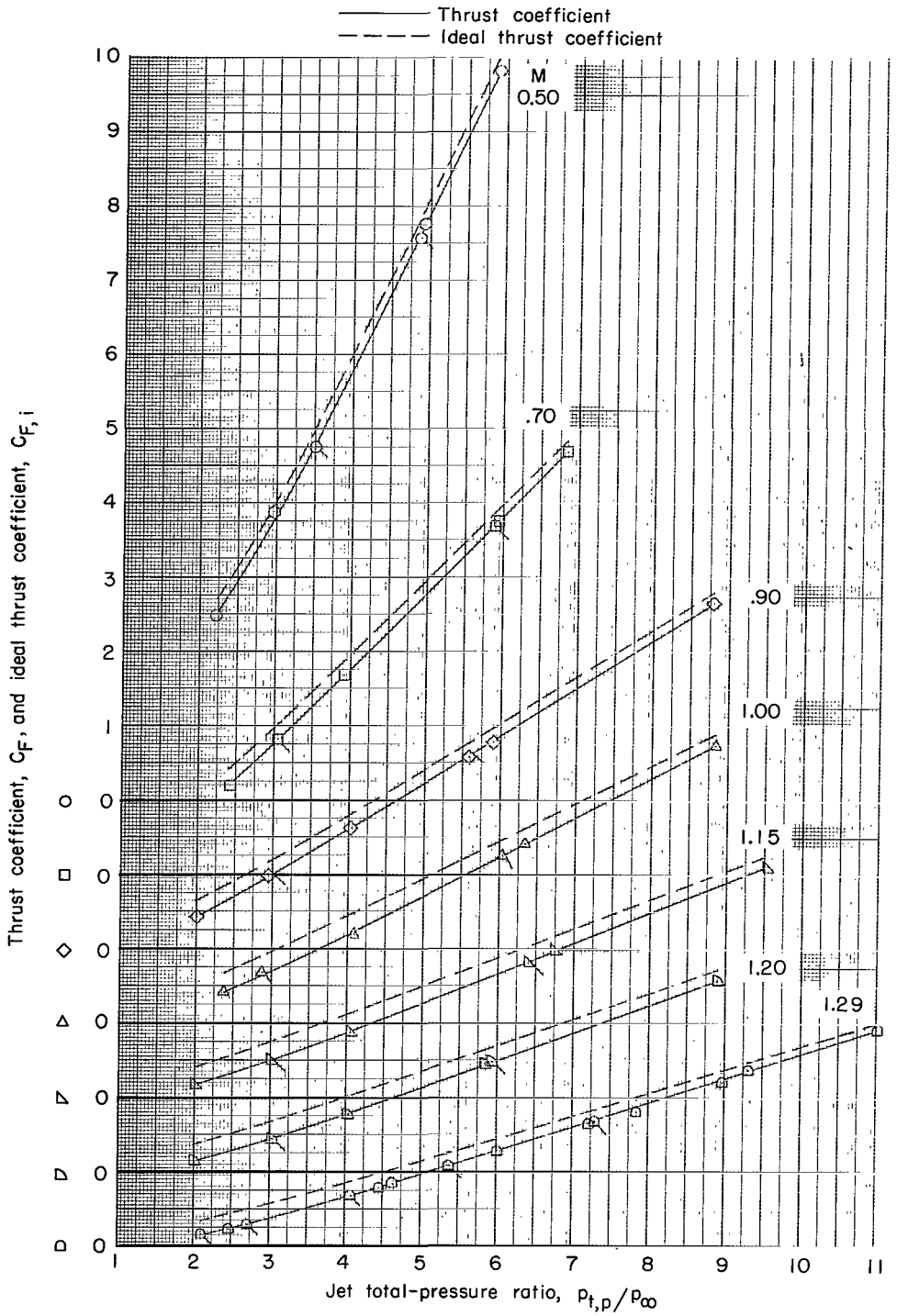

(a) Configuration 1.

Figure 12.- Variation of thrust coefficient and ideal thrust coefficient with jet total-pressure ratio for various Mach numbers. Flagged symbols indicate decreasing pressure ratios.

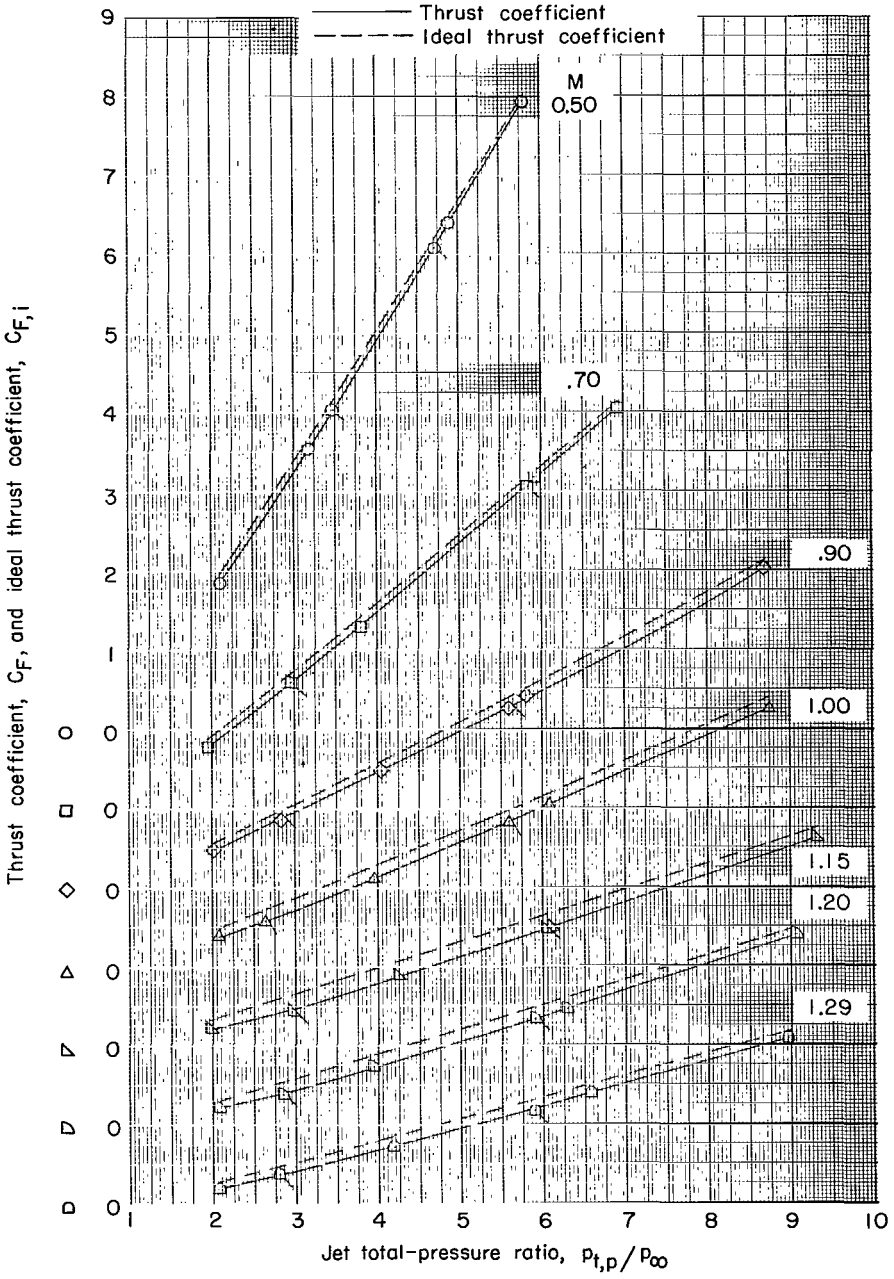

(b) Configuration 2.

Figure 12.- Concluded.

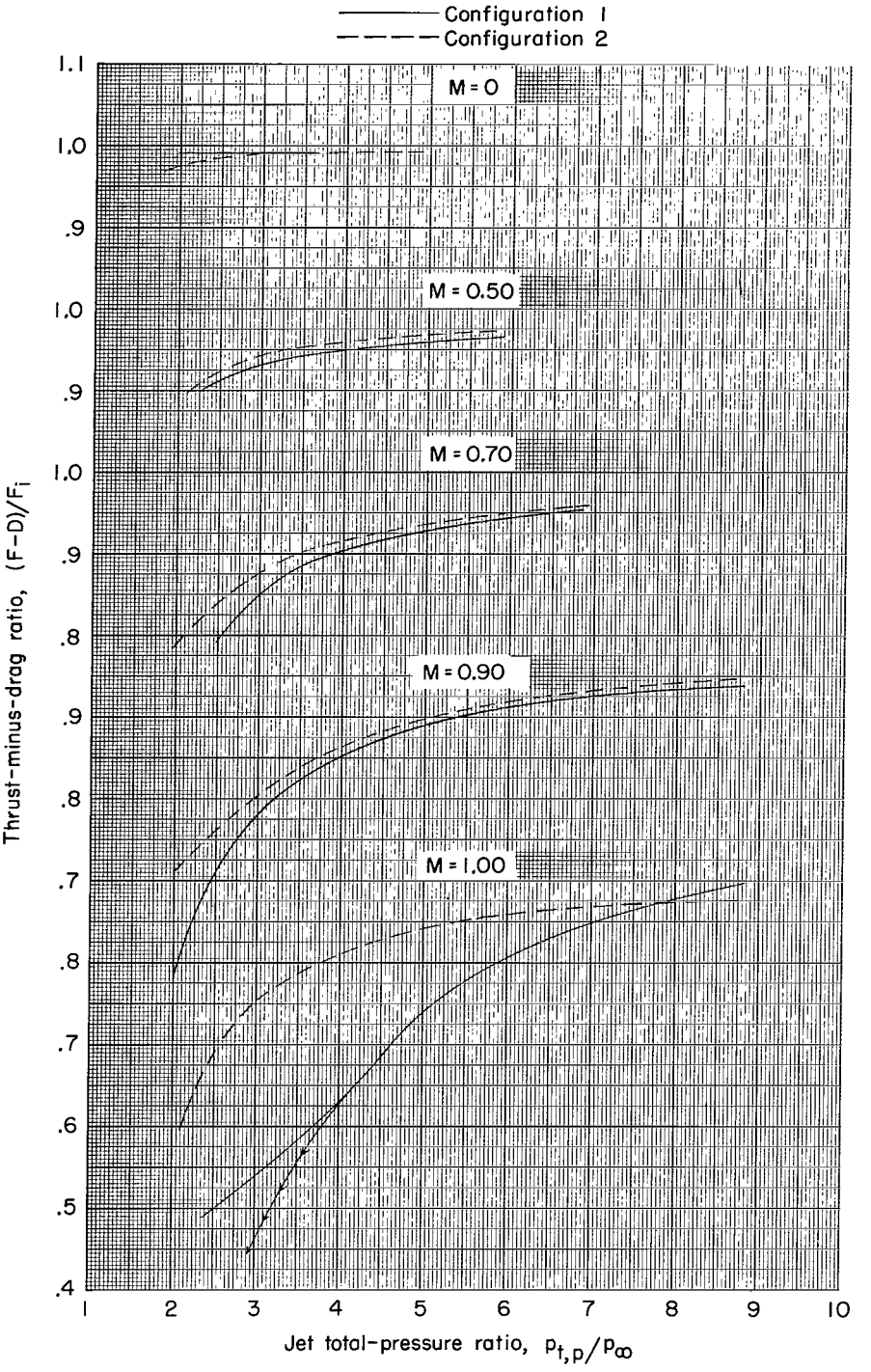

(a) M = 0 and 0.50 to 1.00.

Figure 13.- Variation of thrust-minus-drag ratio with jet total-pressure ratio.

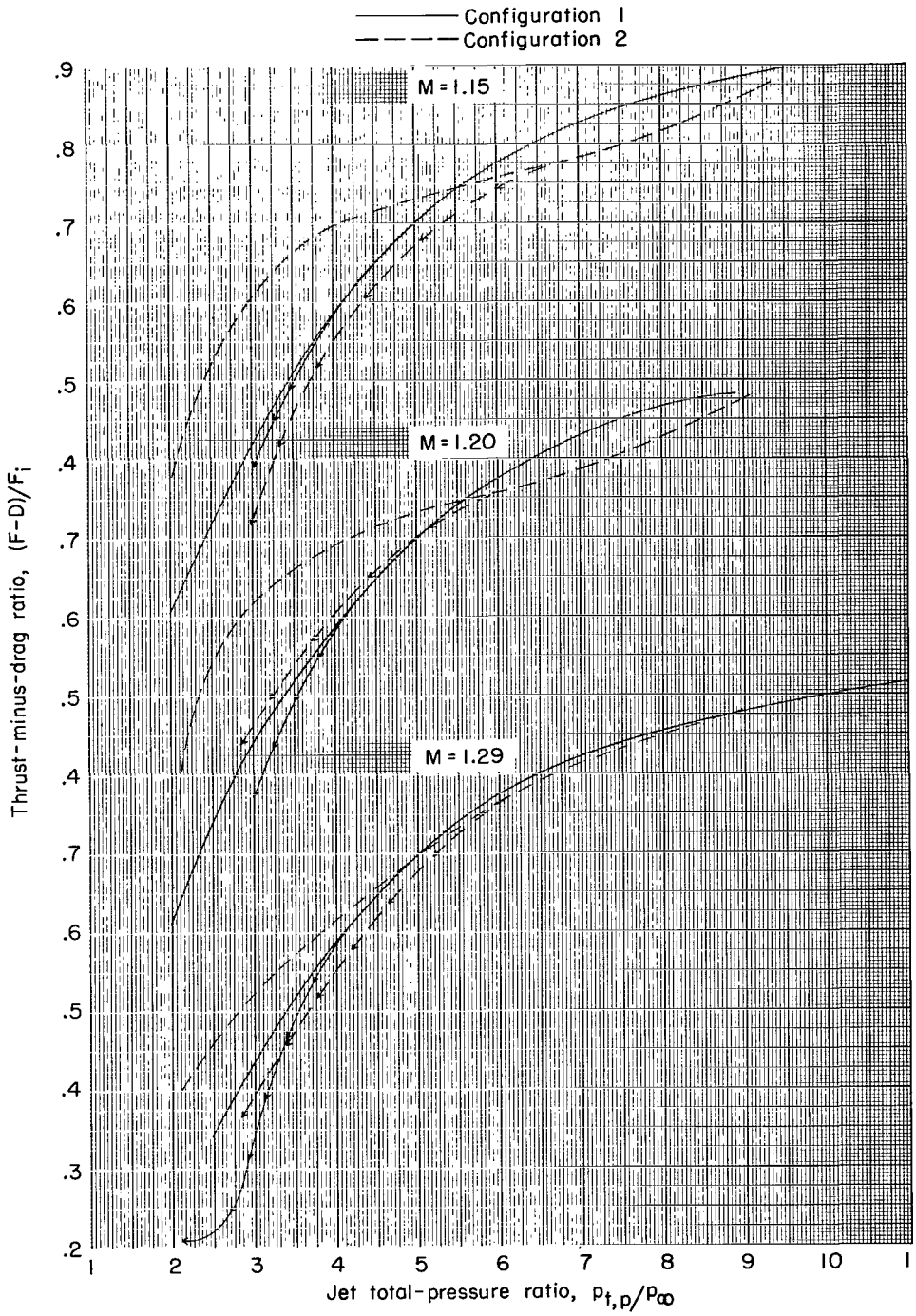

(b) M = 1.15 to 1.29.

Figure 13.- Concluded.

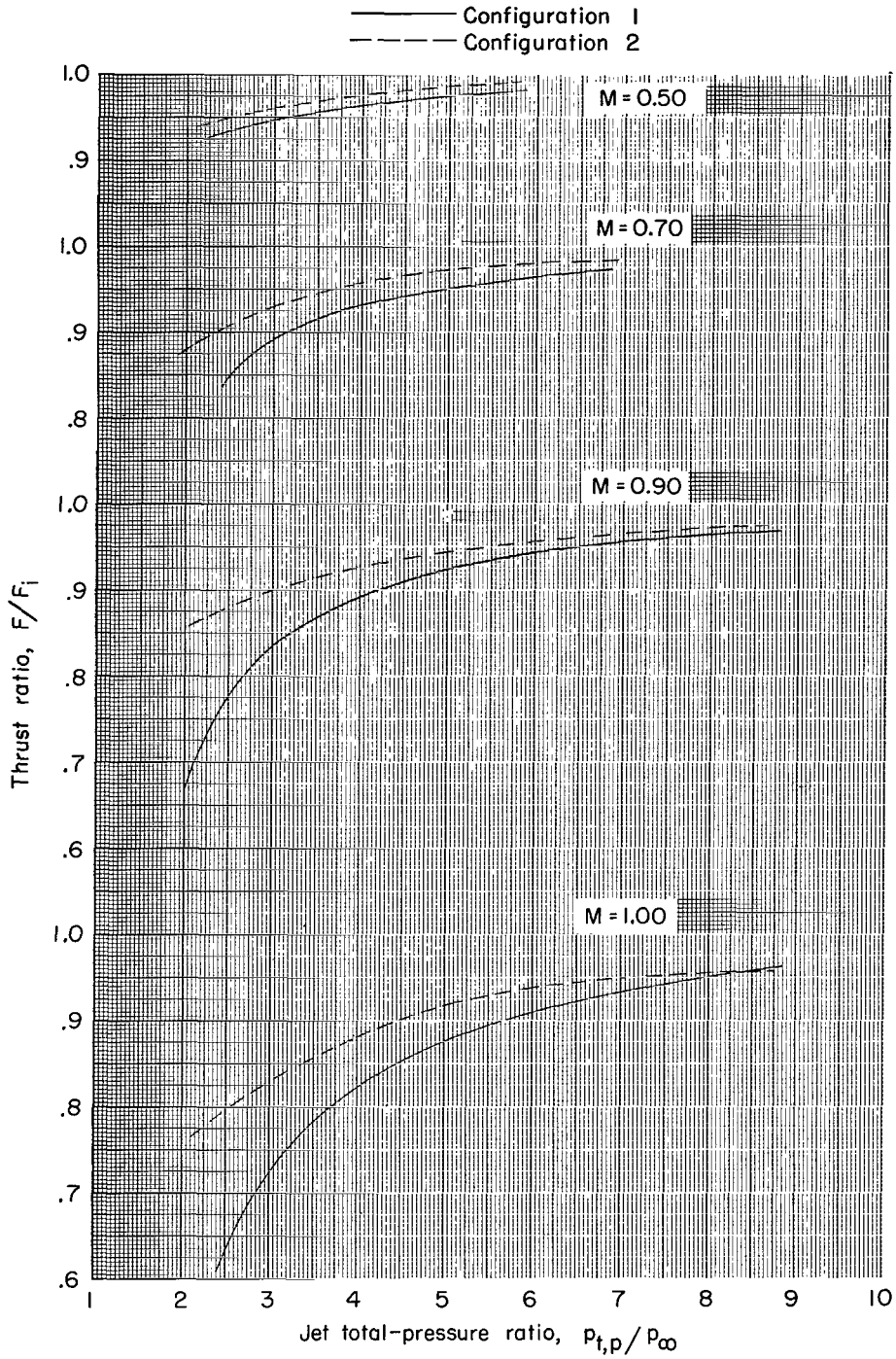

(a) M = 0.50 to 1.00.

Figure 14.- Effect of jet total-pressure ratio on thrust ratio.

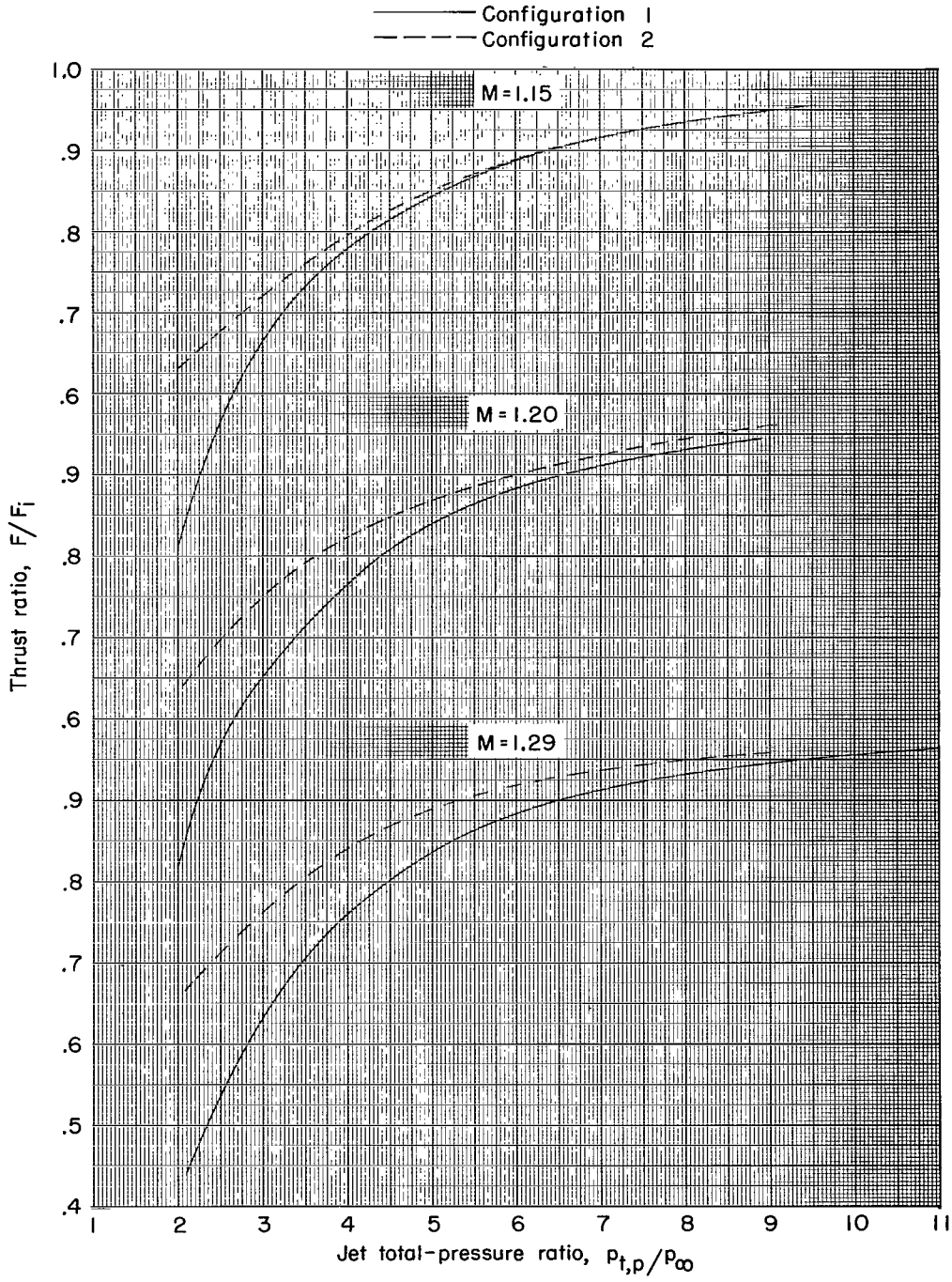

(b) M = 1.15 to 1.29.

Figure 14.- Concluded.

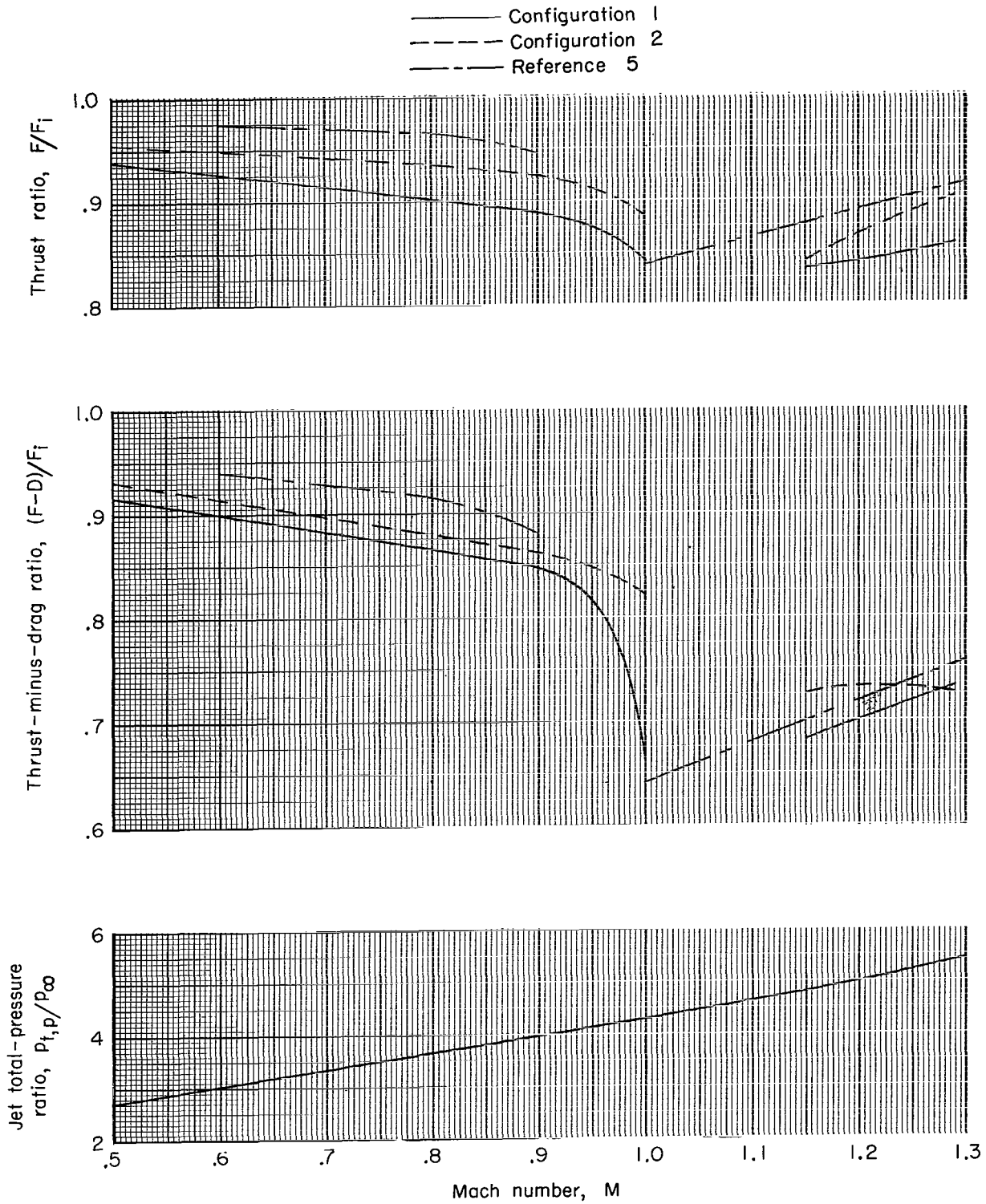

Figure 15.- Variation of thrust-minus-drag and thrust ratio with Mach number for jet total-pressure-ratio schedule.

"The aeronautical and space activities of the United States shall be conducted so as to contribute . . . to the expansion of human knowledge of phenomena in the atmosphere and space. The Administration shall provide for the widest practicable and appropriate dissemination of information concerning its activities and the results thereof."

—NATIONAL AERONAUTICS AND SPACE ACT OF 1958

NASA SCIENTIFIC AND TECHNICAL PUBLICATIONS

TECHNICAL REPORTS: Scientific and technical information considered important, complete, and a lasting contribution to existing knowledge.

TECHNICAL NOTES: Information less broad in scope but nevertheless of importance as a contribution to existing knowledge.

TECHNICAL MEMORANDUMS: Information receiving limited distribution because of preliminary data, security classification, or other reasons.

CONTRACTOR REPORTS: Technical information generated in connection with a NASA contract or grant and released under NASA auspices.

TECHNICAL TRANSLATIONS: Information published in a foreign language considered to merit NASA distribution in English.

TECHNICAL REPRINTS: Information derived from NASA activities and initially published in the form of journal articles.

SPECIAL PUBLICATIONS: Information derived from or of value to NASA activities but not necessarily reporting the results of individual NASA-programmed scientific efforts. Publications include conference proceedings, monographs, data compilations, handbooks, sourcebooks, and special bibliographies.

Details on the availability of these publications may be obtained from:

SCIENTIFIC AND TECHNICAL INFORMATION DIVISION

NATIONAL AERONAUTICS AND SPACE ADMINISTRATION

Washington, D.C. 20546